# Linear rheology of reversibly cross-linked biopolymer networks

Henry E. Amuasi, Andreas Fischer, Annette Zippelius, and Claus Heussinger

Citation: The Journal of Chemical Physics **149**, 084902 (2018); doi: 10.1063/1.5030169
View online: https://doi.org/10.1063/1.5030169
View Table of Contents: http://aip.scitation.org/toc/jcp/149/8
Published by the American Institute of Physics

# Linear rheology of reversibly cross-linked biopolymer networks

Henry E. Amuasi, Andreas Fischer, Annette Zippelius, and Claus Heussinger[a)]
*Institute of Theoretical Physics, Georg-August University of Göttingen, 37073 Göttingen, Germany*

(Received 20 March 2018; accepted 8 August 2018; published online 24 August 2018)

We suggest a simple model for reversible cross-links, binding, and unbinding to/from a network of semiflexible polymers. The resulting frequency dependent response of the network to an applied shear is calculated via Brownian dynamics simulations. It is shown to be rather complex with the time scale of the linkers competing with the excitations of the network. If the lifetime of the linkers is the longest time scale, as is indeed the case in most biological networks, then a distinct low frequency peak of the loss modulus develops. The storage modulus shows a corresponding decay from its plateau value, which for irreversible cross-linkers extends all the way to the static limit. This additional relaxation mechanism can be controlled by the relative weight of reversible and irreversible linkers. *Published by AIP Publishing.* https://doi.org/10.1063/1.5030169

## I. INTRODUCTION

The simulation of filamentous polymer networks (e.g., cytoskeletal networks) presents a substantial challenge as to the broad spectrum of length-scales and relaxation times.[1] At high frequencies, the response is governed by small-wavelength bending fluctuations of individual filaments. The higher the driving frequency, the smaller the dominant wavelength, which leads to the well-known frequency-dependence for the modulus $G \sim \omega^{3/4}$.[2,3] At intermediate frequencies, collective network modes come into play and the response is mainly elastic.[4] Different theories have been devised to understand this regime.[5–7] The low frequency regime of the modulus is sensitive to the dynamics of the cross-linking proteins. If these provide permanent connections and are sufficiently numerous for the network to percolate, then the low frequency limit is characterized by a finite elastic modulus.[8] However, cross-links in biological networks usually have a lifetime $\tau_{\mathrm{cl}}$ of only several seconds[9,10] so that the network can undergo a terminal relaxation at frequencies $\omega < 1/\tau_{\mathrm{cl}}$. In this low-frequency regime, the network flows like a liquid, e.g., governed by filament reptation and constraint release[11] in entangled networks or repeated cross-link un/rebinding processes in cross-linked networks.[12–14]

While there are ample simulations dealing with intermediate and high frequencies,[15–20] efforts to combine the entire frequency range in one simulation are scarce.[21,22] Here we present an alternative approach. With the high-frequency branch being well understood, we sacrifice high-frequency bending fluctuations of individual filaments, treating the filaments with the help of an effective potential of mean force. A similar approach was first described in two-dimensional Mikado networks in Ref. 23. Our three-dimensional simulations are built on the method of Huisman *et al.*[15] and Amuasi *et al.*[17] Within this approach, we study in detail the process of reversible cross-linking and its role for the rheological response of the filament network to small angle oscillatory shear.

## II. MODEL

We study the frequency dependent visco-elastic response of a randomly cross-linked biopolymer network. It is our aim to work out and understand the differences between reversibly and irreversibly bound cross-links. To this end, we simulate the Brownian dynamics of randomly cross-linked filament networks, treating the positions of the cross-links as dynamical variables.

The polymer segments represent connections between neighboring cross-links and thus mediate interactions between them. We ignore the precise configurations of the polymer segments and instead work with effective spring-like interactions between the cross-links. This approximation is well justified for low frequencies, where the short wavelength modes of the polymer segments are relaxed.

To account for reversible cross-link binding, we also allow the polymer segment length in between cross-links to vary. In this model, a cross-link unbinding/rebinding event is treated as the diffusion of the cross-link along the filament. Polymer-mediated forces acting on the cross-link then act as bias to this diffusion process. This type of description is useful to understand the limiting case of fast un-binding and rebinding. The opposite limit of slow binding has to be dealt with by stochastic transitions modeled with the help of appropriate Metropolis Monte Carlo steps.

We model the effective polymer-mediated interactions between the cross-links at positions $\{\mathbf{r}_i\}_{i=1}^{N}$ by

$$H = \sum_{ij} k_2^{(ij)} (|\mathbf{r}_{ij}| - l_{(ij)})^2 + \sum_{ijk} k_3^{(ijk)} \theta_{ijk}^2. \tag{1}$$

The first term represents the polymer stretching energy with stiffness $k_2^{(ij)} = \alpha / l_{ij}$. Here $l_{ij}$ is the contour length between cross-link $i$ and $j$. The parameter $\alpha$ is a constant that, in the

a)Author to whom correspondence should be addressed: heussinger@theorie.physik.uni-goettingen.de

context of athermal beam stretching, takes the meaning of Young's modulus multiplied by the cross sectional area. The second term in Eq. (1) represents the polymer bending energy, restraining the angle, $\cos\theta_{ijk} = \hat{\mathbf{r}}_{ij}\cdot\hat{\mathbf{r}}_{jk}$, between any three consecutive cross-links $ijk$ along the same polymer. The bending stiffness is taken to be $k_3^{(ijk)} = \frac{3}{2}k_BTl_p/(l_{ij}+l_{jk})$. The scale for the bending stiffness is set by temperature $k_BT$ and the persistence length of the polymer $l_p$. For more information on the model Hamiltonian, see Ref. 17.

We assume the network to be embedded in a viscous fluid of viscosity $\eta$, giving rise to viscous drag and thermal noise. In the overdamped limit, the cross-links perform Brownian motion, described by a Langevin equation

$$\eta\dot{\mathbf{r}}_i = \mathbf{F}_i + \boldsymbol{\xi}_i. \tag{2}$$

The systematic force is given by $\mathbf{F}_i = \partial H/\partial\mathbf{r}_i$ and the noise is chosen according to the fluctuation dissipation theorem (FDT) with zero mean and variance $\langle\boldsymbol{\xi}_i(t)\cdot\boldsymbol{\xi}_j(t')\rangle = 2k_BT\eta\,\delta_{ij}\delta(t-t')$.

Physiological cross-linking proteins can unbind thermally or under the application of mechanical forces since the bonds they form are rather weak. Here we present a model for the cross-link unbinding process that incorporates both thermal and forced unbinding. In both cases, we assume that—after unbinding—the cross-link immediately rebinds to the filament, possibly at another nearby location. In this "fast-rebinding" limit, we arrive at a description of cross-link binding in terms of a biased diffusion process.

A cross-link may be regarded as a spring with two heads, each of which is binding to a different filament (see Fig. 1). With respect to cross-link binding, a filament can be considered as a periodic energy landscape along its arc length $s$, the minima of which represent the binding sites. The double-helical shape of F-actin suggests a periodicity of $\delta \approx 50$ nm. We model a thermal unbinding event as an activation process with rate $k = \tilde{k}_0 e^{-\beta\Delta E}$.

Remembering that the heads of the cross-link are coupled via a spring, one has to account for the additional force $\mathbf{F}^{cl}$ on a head, arising when the spring is stretched or compressed. We assume that the unbinding kinetics is determined by the component $F_\parallel^{cl}$ parallel to the local tangent of the polymer: the jump rate in the direction of $F_\parallel^{cl}$ is enhanced and decreased in the opposite direction (see Fig. 1), which breaks the symmetry of the force-free case. Assuming $F_\parallel^{cl}$ is pointing to the right, this changes the jump rates to

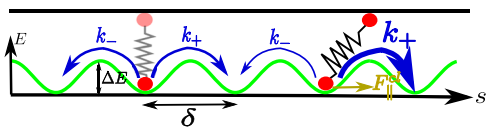


FIG. 1. Scheme of the unbinding process: For a cross-link (depicted as a spring with two heads), a filament corresponds to a periodic energy landscape with periodicity $\delta$ (green) along the filament's arclength $s$. Energy minima represent cross-link binding sites. Unbinding corresponds to a jump over the energy barrier $\Delta E$ to the next minimum. Left: symmetric jump rates $k_+$, $k_-$ (force-free) and right: asymmetric rates (due to the force $F_\parallel^{cl}$ from the spring).

$$k_+ = \tilde{k}_0 e^{-\beta(\Delta E - F_\parallel^{cl}\delta)}, \quad k_- = \tilde{k}_0 e^{-\beta(\Delta E + F_\parallel^{cl}\delta)}. \tag{3}$$

The rate-asymmetry leads to an effective movement of the cross-link-head along the polymer, which can be described by a master equation for the probability $P_s(t)$ to find the cross-link at the binding site $s$ at time $t$,

$$\partial_t P_s(t) = k_+ P_{s-1}(t) + k_- P_{s+1}(t) - (k_+ + k_-)P_s(t). \tag{4}$$

Multiplying the above equation by $s$ and summing over all $s$, we find an equation for the average velocity of the cross-link,

$$v_s := \partial_t \sum_s sP_s(t)\delta = 2k_0\delta\sinh(\beta\delta F_\parallel^{cl}), \tag{5}$$

with $k_0 = \tilde{k}_0 e^{-\beta(\Delta E)}$. Assuming a small pulling force so that linear response applies, the equation of motion reads explicitly

$$\zeta v_s = F_\parallel^{cl} + \xi. \tag{6}$$

Here $\zeta = k_BT/(2k_0\delta^2)$ denotes the mobility, related to the diffusion constant $D_{cl} = 2k_0\delta^2$ in the usual way, and we have added a noise term with $\langle\xi(t)\rangle = 0$ and

$$\langle\xi(t)\xi(t_0)\rangle = 2k_BT\zeta\,\delta(t-t_0). \tag{7}$$

The spring is stretched or compressed due other cross-links connecting to the two filaments under consideration (see Fig. 2). The forces acting on the 2 heads of the motor at positions $\mathbf{r}_{2a}$ and $\mathbf{r}_{2b}$,

$$\begin{aligned}\eta\dot{\mathbf{r}}_{2a} &= \mathbf{F}_{2a} + \mathbf{F}^{cl},\\ \eta\dot{\mathbf{r}}_{2b} &= \mathbf{F}_{2b} - \mathbf{F}^{cl},\end{aligned} \tag{8}$$

are decomposed into the forces due to the other cross-links, $\mathbf{F}_{2a}$ and $\mathbf{F}_{2b}$, and the force, $\mathbf{F}^{cl}$, due to the springlike cross-link, considered explicitly.

For the simulations, we consider the cross-link as pointlike, and thus the two heads of the cross-link are at identical positions, which can be achieved approximately by a high spring constant for the cross-link. In this limit, the two heads move with the same velocity so that Eq. (8) can be solved for $\mathbf{F}^{cl} = (\mathbf{F}_{2b} - \mathbf{F}_{2a})/2$. The equations of motion for the two heads of the cross-link connecting filaments $a$ and $b$ then read

$$\zeta v_{2a} = F_\parallel^a + \xi_a, \tag{9}$$

$$\zeta v_{2b} = F_\parallel^b + \xi_b, \tag{10}$$

giving rise to a change in arclength $\dot{l}_{12} = -\dot{l}_{23} = v_{2a}$ and $\dot{l}_{42} = -\dot{l}_{25} = v_{2b}$. We approximate the local tangent as $F_\parallel^a = \mathbf{F}^{cl}\cdot(\mathbf{r}_3 - \mathbf{r}_1)/|\mathbf{r}_3 - \mathbf{r}_1|$ and correspondingly for $F_\parallel^b$.

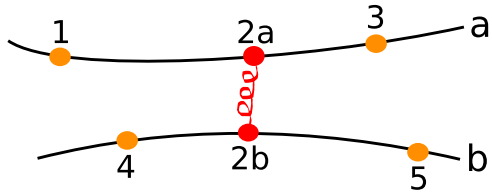


FIG. 2. Cross-link modeled as a spring embedded in a network with adjacent cross-links (pointlike), labeled 1,3,4,5.

In turn, a changing arclength $l_{(ij)}$ modifies the spring constants in Eq. (1) and thus the forces acting on the cross-links. This mechanism provides the coupling between the spatial (lab-frame) degrees of freedom $\mathbf{r}_i$ of the cross-links and the internal degrees of freedom $s_a$, measured by the position along the filament.

### A. Technical details

As units, we choose $l_p$, $k_BT$, and $\eta$. In these units, the parameter $\alpha$ is taken as $\alpha = 349$, which is motivated by the comparison of a spring constant of a beam with that of a wormlike chain.

We simulate 1000 cross-links on 300 filaments each of length 1.28 in a simulation box, which is taken to be of length 1. Periodic boundary conditions are assumed. To incorporate shear deformations, we use the method of Lee and Edwards. To measure the frequency-dependent modulus, we apply a shear strain $\gamma = \gamma_0 \sin(\omega t)$ with frequency $\omega$ and $\gamma_0 = 0.008\ldots0.16$ depending on frequency. The resulting stress is fitted to the form $\sigma = \gamma_0(G' \sin(\omega t) + G'' \cos(\omega t))$, which defines the real and imaginary part of the complex modulus $G(\omega) = G'(\omega) + iG''(\omega)$. In order to prevent two cross-links to collapse into a single point, we implemented a minimum distance $l_{\min} = 0.1 l_p$ between two neighboring cross-links on a filament via the repulsive part of a Lennard-Jones potential.

## III. RESULTS: IRREVERSIBLE CROSS-LINKS

We first discuss irreversible cross-links, i.e., the limit $\zeta/\eta \to \infty$. The measured complex shear modulus $G(\omega)$ of the network is depicted in Fig. 3 over eight orders of magnitude in frequency.

Comparing with data from the literature, one immediately recognizes the absence of the typical high-frequency branch $G \sim (i\omega)^{3/4}$. The reason for this is the coarse-graining procedure intrinsic in our simulation method. The scaling with 3/4 derives from the competition between the driving frequency and time scale of the relaxation of bending modes with wavelength below the inter-cross-link distance. In our simulation, all these modes are assumed equilibrated, and thus no such competition exists. As explained in the Introduction, this simplification allows us to increase the time scale of the simulation to put the emphasis on low-frequency phenomena, like cross-link binding.

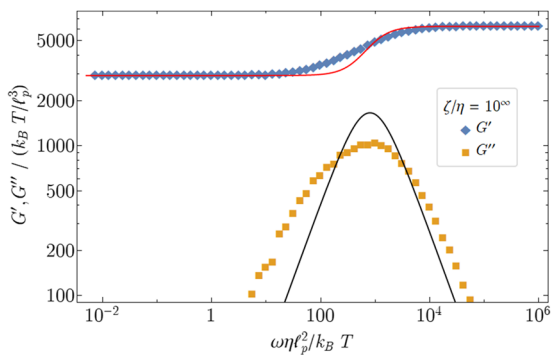


FIG. 3. Storage and loss modulus of a network with permanent cross-links. The solid lines represent a fit to the model of Eq. (11).

The storage modulus shows two plateaus with a transition region at $\omega_c \approx 10^3$. Associated with this transition is a maximum in the loss modulus $G''$. In the low-frequency plateau, the loss modulus scales as $G'' \sim \omega$ and as $G'' \sim \omega^{-1}$ in the high-frequency plateau. The crossover frequency $\omega_c$ corresponds to typical time scales on the length-scale of the inter-cross-link distance $l_c \approx 0.1 l_p$. For bending modes, this time scale is given by $1/\tau_b \sim k_BT l_p/l_c^3\eta \sim 10^3$ in the units used in the figure. The typical time scale for stretching modes is similar, $1/\tau_s \sim EA/l_c\eta \sim 3{\cdot}10^3$.

As the shear flow of the fluid mainly couples to the stretching modes, the high-frequency response is dominated by filament stretching, when viscous stresses force the filaments to follow the fluid flow. At lower frequencies, these stretching modes can relax and the filaments deform mainly via bending. We have checked by running additional simulations with modified stretching and bending stiffness that the modulus is indeed dominated by stretching at high frequencies and by bending at low frequencies.[24] In other words, the real part of the modulus in the high-frequency plateau is proportional to the stretching stiffness of the filaments, while the modulus in the lower plateau is proportional to the bending stiffness.

A simple harmonic one-degree of freedom model can reproduce this behavior: consider a particle coupled to two springs with spring constants $k_1$ and $k_2$, respectively. One of the springs is driven by an external force that periodically changes the length $L(t)$. The particle itself is coupled viscously to this force via $\dot{L}$. The equation of motion thus reads

$$\eta(\dot{x} - \dot{L}) = k_2(L - x) - k_1 x, \tag{11}$$

which is easily solved for $x(t)$ assuming $L(t) = L_0 e^{i\omega t}$. Real and imaginary parts of the amplitude of oscillation are reproduced as solid lines in Fig. 3. At high frequencies, above $1/\tau_1 = (k_1 + k_2)/\eta$, the oscillation amplitude reaches a plateau at $\Re x = L_0$ ($\Re x$ being the real part of $x$), and thus the particle follows the external driving with the same amplitude. Both springs contribute to the response. For the network, this corresponds to the stretching dominated high-frequency plateau. Lowering the frequency below $1/\tau_1$, the particle can relax from the high amplitudes and $\Re x$ is reduced. Finally, at small frequencies below $1/\tau_2 = \sqrt{k_1 k_2}/\eta$, the plateau reaches the lower asymptotic value $\Re x = L_0 k_2/(k_1 + k_2)$. In this limit, the particle relaxes such that the load on the spring $k_1$ is reduced. In the network, this corresponds to the relaxation of the stretching deformations such that only bending deformations remain. It is clear from the figure that the peak width from the network simulations is broader than the single Maxwellian peak from the simple toy model. This is to be expected given a broad spectrum of relaxation times in the network, as compared with the two times scales $\tau_1$ and $\tau_2$ in the model.

We conclude that the linear response of the network to an imposed frequency dependent strain can be divided into 3 regimes. For the smallest frequencies, all excitations are allowed to relax, giving rise to a constant storage modulus

whose value is dominated by bending modes. For an intermediate range of frequencies, corresponding to typical frequencies of the spectrum of the network, the loss modulus displays a peak, while the storage modulus increases. For the highest frequencies beyond the spectrum of the network, the loss modulus goes to zero, while the storage modulus is constant. Its plateau value scales like the stretching stiffness. This interplay between bending and stretching and non-affine and affine response has received a lot of attention recently (for a review see Ref. 7). Here we are mainly concerned with the effect of cross-link binding, which is what we turn to in Sec. IV.

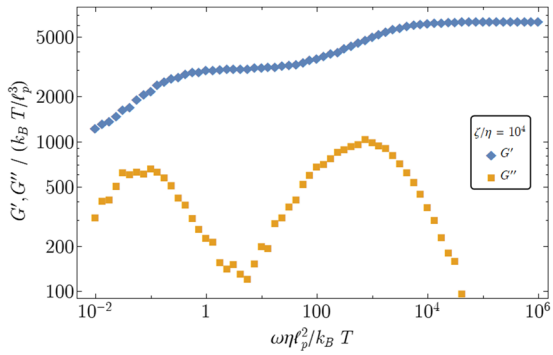


FIG. 4. Storage and loss modulus as a function of frequency for a network with reversible cross-links. The friction coefficient for cross-link sliding is taken as $\zeta/\eta = 10^4$.

## IV. RESULTS: REVERSIBLE CROSS-LINKS

We now turn to the discussion of the rheology of networks with reversible cross-links, characterized by a finite time constant $\zeta$. As compared to the irreversible case, we expect to see a further decrease of the storage modulus at small frequencies corresponding to the additional relaxation mechanism of sliding cross-links. This is indeed observed in Fig. 4.

The storage modulus is seen to display three distinct plateaus: the stretching dominated high frequency plateau, the bending dominated one at intermediate frequencies—both present also in the irreversible case—and an additional low frequency plateau (also see Fig. 5). The latter is finite because the cross-links only slide along the filament and do not unbind. Also the end-links are assumed to be non-sliding. We expect this plateau to vanish, if the cross-links also unbind, so that a complete relaxation of the network becomes possible. The loss modulus displays two distinct peaks, one corresponding to a characteristic network frequency (as discussed above) and the other one to the inverse relaxation time of a cross-link.

The time scale for cross-link sliding is obtained as $1/\tau_{\rm sl} \sim k_B T l_p/\zeta l_c^3$ (which is ~0.1 in the figure). Thus, we expect the sliding relaxation to set in at a typical frequency $\omega_{sl} \sim 1/\tau_{sl} \sim 1/\zeta$. In order to test this scaling, we show results for different values of $\zeta$ in Fig. 5. The terminal relaxation and the peak in the loss modulus indeed shift with $\zeta$ to smaller frequencies. The particular scaling with $1/\zeta$ is highlighted in Fig. 6, where the frequency axis is rescaled by a factor $\omega_{sl}$. In particular, the low-frequency wing is seen to scale with the cross-link time scale $\sim \zeta$, whenever there is a clear time scale separation between network relaxation processes (governed by $\eta$) and cross-link sliding (governed by $\zeta$). In this regime, the loss modulus scales as $G'' \sim \zeta\omega$ indicating viscous behavior with the viscosity set by the cross-link sliding constant $\zeta$.

The scaling collapse at low frequencies breaks down for the case $\zeta/\eta = 1$ (blue diamonds). For this data set, both viscous processes are indistinguishable and occur on similar time scales. This explains the lack of scaling of these data in Fig. 6.

Further manipulation of the low-frequency plateau can be achieved by having both, reversible and permanent, cross-links in a network. Figure 7 displays the modulus for networks with a total of $N_{\rm cl} = 1000$ cross-links, a varying fraction of which are reversible. Reducing the reversible fraction, the peak height at low frequencies in $G''$ is reduced. We find that the peak height scales with the number of reversible cross-links, $G''_{\rm peak} \sim N_{\rm rev}$. At the same time, the low-frequency plateau in $G'$ increases. Recent calculations[25] show that the network should undergo a rigidity percolation transition as the fraction of reversible cross-links is increased. At this point, the remaining network (made from the permanent cross-links) becomes fluid and is no longer able to build up forces to resist the imposed deformation. Our data show this trend: The bending dominated plateau of the shear modulus, which persists up to the smallest frequencies for $N_{\rm rev} = 0$, decays more and more rapidly as the fraction of reversible cross-links is increased. However, the storage modulus does not decay completely. Instead a low-frequency plateau is observed in our simulations—even when

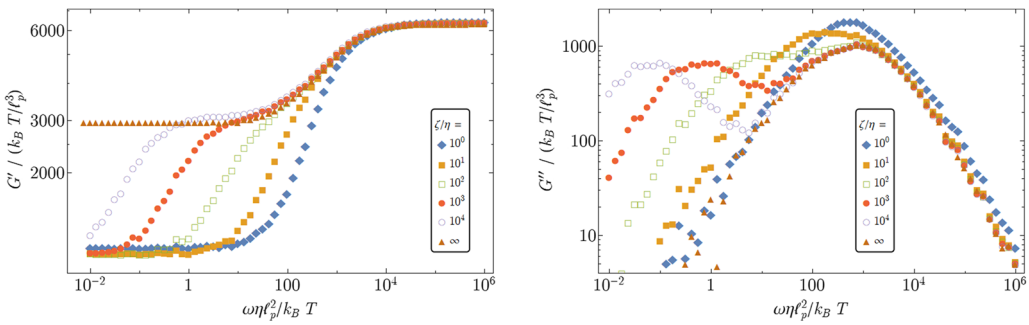


FIG. 5. Storage and loss modulus as a function of frequency for several values of $\zeta/\eta$.

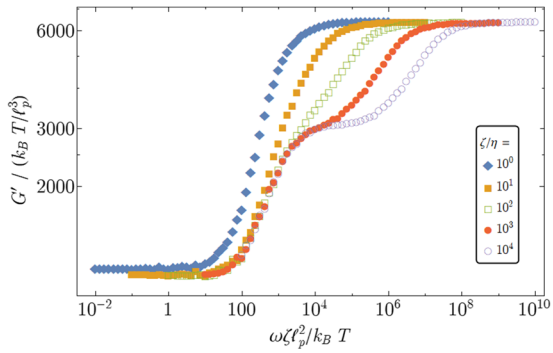


FIG. 6. Storage modulus as a function of frequency for several values of $\zeta/\eta$. Frequency is scaled with $\zeta$; see text for details.

all cross-links are reversible. As discussed above, the reason for this regime is the fact that in our simulations, the cross-links cannot fully relax and are constrained to stay on the filaments for all times. This inhibits the full fluidization of the sample. Other effects which can cause small, but finite rigidity even below rigidity percolation are thermal fluctuations[26] and prestresses,[27] both of which are present in our simulations.

In experiments on reconstituted actin networks (e.g., Ref. 14), an important control parameter is the degree of (reversible) cross-linking, measured by $R = c_x/c_a$, the ratio of the cross-link to actin monomer density. We implement this parameter by changing the number of connections per filament. In the above discussed networks, the average connectivity (cross-links $N_c = 1000$ per filament $N_f = 300$) was $n = 2N_c/N_f = 6.67$. We now reduce this number down to $N_c = 400$ or $n = 2.67$ and take all cross-links to be reversible.

The resulting storage and loss moduli are shown in Fig. 8. One observes that here the entire frequency domain is affected by the change of $N_c$ in contrast to the previous scenario (Fig. 7). At high frequencies, the reversible cross-links behave just like permanent links and the network feels the reduced connectivity of the filaments. The reason for the reduction of the modulus is that with fewer cross-links, filament segments become longer and therefore softer.

The low-frequency bending-dominated plateau is more strongly affected than the high-frequency stretching-dominated plateau because bending stiffness is more sensitive to segment length $l_c$, $k_b \sim 1/l_c^3$, as compared to the stretching stiffness $k_s \sim 1/l_c$. This difference is emphasized in the inset of Fig. 8(a), where we plot the bending-dominated plateau, $G^*$, together with the stretching dominated plateau as a function of connectivity. Similar results have been obtained by Huisman and Lubensky[27] in the context of an athermal model. Parameters are slightly different, however. In our simulations we go closer toward the percolation threshold, which also makes the system more likely to experience finite-size effects.

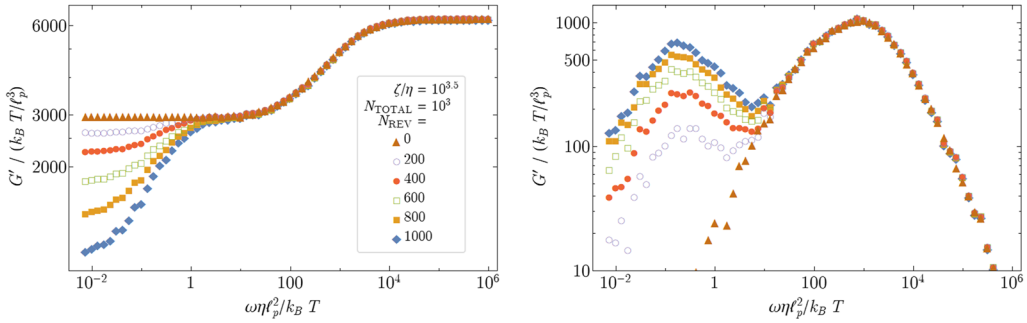


FIG. 7. Storage and loss modulus as a function of frequency for a network with a fixed total number of cross-links, $N_{\mathrm{cl}} = N_{\mathrm{perm}} + N_{\mathrm{rev}} = 1000$, and changing number of $N_{\mathrm{rev}}$.

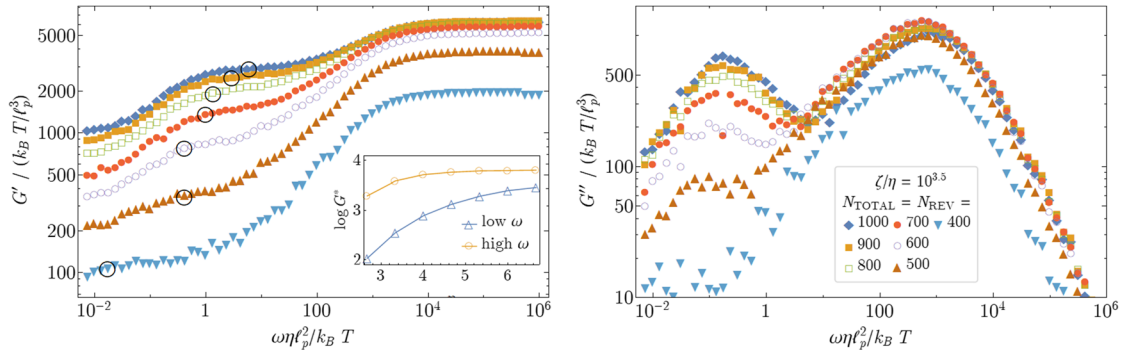


FIG. 8. Storage and loss modulus as a function of frequency for several values of $N_{\mathrm{rev}} = 400, \ldots, 1000$. Inset: plateau modulus as a function of cross-links per filament $n$, extracted from the high-frequency (stretching-dominated) and the intermediate-frequency (bending-dominated) plateau of the storage modulus. The latter value is illustrated by the open black circles.

The low-frequency peak in the loss modulus is strongly degraded when the connectivity is lowered, whereas the high-frequency peak remains nearly unchanged for most of the parameter range investigated. For the lowest connectivity per filament, $n = 2.67$, hardly any relaxation due to sliding cross-links occurs. This is not surprising: Two cross-links at the two ends of a filament are always present and are not allowed to slide so that effectively less than one cross-link per filament contributes to relaxation. The low frequency peak in the loss modulus is no longer detectable and the bending plateau in the storage modulus is replaced by a finite, but a small slope.[4,28]

A similar slope is observed in many experiments. It hints at a broadening of the relaxation spectrum when approaching the rigidity threshold.

The low frequency behavior of the loss and storage moduli can be described approximately by a Maxwell model. We use the plateau modulus, $G^*$, depicted in the inset of Fig. 8(a), as energy scale and the associated "Maxwell" time scale $\tau_M = \zeta/G^* l_p$ to rescale both loss and storage moduli. This rescaling, shown in Fig. 9, works quite well if the network is not too close to the percolation threshold. It is apparent from the scaling plot for the storage modulus (the upper part of Fig. 9) that the two networks closest to percolation ($N_{\text{rev}} = 400, 500$) hardly show any terminal relaxation at frequencies $\omega\tau_M < 1$. In these networks, there are only few reversible cross-links per filament and effective filament length is short. Stress relaxation is therefore governed by filament ends, where we have implemented permanent cross-links that (as explained above) are not allowed to unbind. For clarity, we have therefore removed these two networks, when rescaling the loss modulus (lower part of Fig. 9). In the remaining networks, the loss modulus shows nice data collapse in the left wing of the peak. This region is dominated by cross-link (un-)binding. The absence of scaling in the right wing is due to the transition into the second peak of $G''$. It indicates the gradual disappearance of the low-frequency peak within the wing of the high-frequency peak.

As compared with the functional form of a Maxwell model (solid line), the actual peak is broader, quite similar to what is obtained for the high-frequency peak in Fig. 3. Theoretical calculations[25] show that this may be due to network randomness, e.g., binding angles or local mesh-sizes.

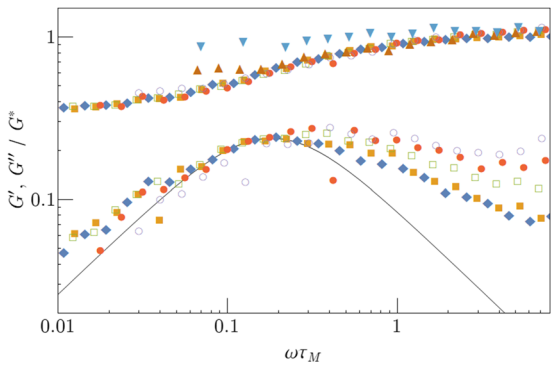


FIG. 9. Storage and loss modulus (data taken from Fig. 8) as a function of frequency and rescaled by the plateau modulus $G^*$ [see inset of Fig. 8(a)] and the associated Maxwell time scale $\tau_M = \zeta/G^* l_p$. Colorcode as in Fig. 8. The solid line compares with the full functional form of a Maxwell model $\sim\omega\tau/((\omega\tau)^2 + 1)$.

## V. CONCLUSION AND OUTLOOK

We have shown that the frequency-dependent elasticity of cross-linked biopolymer networks depends strongly on the dynamics of the cross-links. In our model, we consider thermal as well as forced unbinding of the cross-links in the periodic potential of a filament. In response to an applied strain, the cross-links diffuse along the filaments, thereby partially relaxing stress. If the frequency scale of cross-link motion is sufficiently small as compared to the characteristic energies of the network, a distinct peak appears in the loss modulus at about the sliding frequency. The storage modulus is reduced correspondingly and displays an additional relaxation from the bending dominated plateau, which for permanent cross-links extends down to zero frequency. The additional relaxation at the smallest frequencies can be controlled by the relative weight of mobile to permanent cross-links. The observed softening of the network with an increasing fraction of reversible cross-links indicates the loss of shear rigidity which, however, is not complete since the cross-links cannot completely detach from the filaments. At high frequencies, reversible and permanent cross-links are indistinguishable, only the overall connectivity determines the moduli.

Several extensions of our model are possible. Finite rates for the cross-links to detach and re-attach should be included in a more realistic model of reversible cross-linking. These processes would introduce another time scale and presumably give rise to complete stress relaxation at the lowest frequencies.

So far, we have only considered mobile passive cross-links and focused on their effects on stress relaxation close to equilibrium. A straightforward extension of our work is motors, modeled similar to reversible cross-links but equipped with an active velocity. Motor activity is known to drive the system away from thermal equilibrium, and a simple extension of our model would allow us to study stress relaxation in an active network, which is highly relevant for biological networks as well as of fundamental interest as a model system for nonequilibrium dynamics.

## ACKNOWLEDGMENTS

We acknowledge financial support by the German Science Foundation via the Emmy Noether program (No. He 6322/1-1) as well as the SFB 937 (Project Nos. A1 and A16).

[1] M. J. Unterberger and G. A. Holzapfel, Biomech. Model. Mechanobiol. **13**, 1155 (2014).
[2] G. H. Koenderink, M. Atakhorrami, F. C. MacKintosh, and C. F. Schmidt, Phys. Rev. Lett. **96**, 138307 (2006).
[3] F. Gittes and F. C. MacKintosh, Phys. Rev. E **58**, R1241 (1998).
[4] O. Lieleg, M. Claessens, C. Heussinger, E. Frey, and A. Bausch, Phys. Rev. Lett. **99**, 088102 (2007).
[5] C. Heussinger, B. Schaefer, and E. Frey, Phys. Rev. E **76**, 031906 (2007).
[6] F. C. MacKintosh, J. Käs, and P. A. Janmey, Phys. Rev. Lett. **75**, 4425 (1995).
[7] C. Broedersz and F. MacKintosh, Rev. Mod. Phys. **86**, 995 (2014).
[8] M. L. Gardel, J. H. Shin, F. C. MacKintosh, L. Mahadevan, P. Matsudaira, and D. A. Weitz, Science **304**, 1301 (2004).

[9]O. Lieleg, K. Schmoller, M. Claessens, and A. Bausch, Biophys. J. **96**, 4725 (2009).
[10]A. J. Ehrlicher, R. Krishnan, M. Guo, C. M. Bidan, D. A. Weitz, and M. R. Pollak, Proc. Natl. Acad. Sci. U. S. A. **112**, 6619 (2015).
[11]P. Lang and E. Frey, Nat. Commun. **9**, 494 (2018).
[12]S. M. V. Ward, A. Weins, M. R. Pollak, and D. A. Weitz, Biophys. J. **95**, 4915 (2008).
[13]C. Broedersz, M. Depken, N. Yao, M. Pollak, D. Weitz, and F. MacKintosh, Phys. Rev. Lett. **105**, 238101 (2010).
[14]O. Lieleg, M. Claessens, Y. Luan, and A. Bausch, Phys. Rev. Lett. **101**, 108101 (2008).
[15]E. Huisman, C. Storm, and G. Barkema, Phys. Rev. E **78**, 051801 (2008).
[16]E. Huisman, C. Storm, and G. Barkema, Phys. Rev. E **82**, 061902 (2010).
[17]H. Amuasi, C. Heussinger, R. Vink, and A. Zippelius, New J. Phys. **17**, 083035 (2015).
[18]D. A. Head, A. J. Levine, and F. C. MacKintosh, Phys. Rev. E **68**, 061907 (2003).
[19]P. R. Onck, T. Koeman, T. van Dillen, and E. van der Giessen, Phys. Rev. Lett. **95**, 178102 (2005).
[20]T. Kim, W. Hwang, H. Lee, and R. Kamm, PLoS Comput. Biol. **5**, e1000439 (2009).
[21]C. Cyron, A. R. Bausch, K. W. Müller, and W. A. Wall, J. Comput. Phys. **244**, 236 (2013).
[22]K. W. Müller, R. F. Bruinsma, O. Lieleg, A. R. Bausch, W. A. Wall, and A. J. Levine, Phys. Rev. Lett. **112**, 238102 (2014).
[23]C. Heussinger and E. Frey, Phys. Rev. E **75**, 011917 (2007).
[24]A. Fischer, "Viscoelasticity of transiently cross-linked biopolymer networks," M.S. thesis, University Göttingen, 2016.
[25]J. Plagge, A. Fischer, and C. Heussinger, Phys. Rev. E **93**, 062502 (2016).
[26]M. Dennison, M. Sheinman, C. Storm, and F. C. MacKintosh, Phys. Rev. Lett. **111**, 095503 (2013).
[27]E. M. Huisman and T. C. Lubensky, Phys. Rev. Lett. **106**, 088301 (2011).
[28]O. Lieleg and A. R. Bausch, Phys. Rev. Lett. **99**, 158105 (2007).